Journal of ELECTRONIC MATERIALS, Vol. 49, No. 1, 2020
https://doi.org/10.1007/s11664-019-07743-0

Near-Net-Shape Fabrication of Thermoelectric Legs by Flash Sintering

MASASHI MIKAMI,[1,4] YOSHIAKI KINEMUCHI,[1] KAZUYA KUBO,[2] NAOKI UCHIYAMA,[2] HIDETOSHI MIYAZAKI,[3] and YOICHI NISHINO[3]

1.—National Institute of Advanced Industrial Science and Technology, 2266-98 Anagahora, Shimoshidami, Moriyama, Nagoya 463-8560, Japan. 2.—Atsumitec Co., Ltd., 7111 Ubumi, Yuto, Nishi, Hamamatsu 431-0192, Japan. 3.—Nagoya Institute of Technology, Gokiso, Syowa, Nagoya 466-8555, Japan. 4.—e-mail: m-mikami@aist.go.jp

This study examines the near-net-shape fabrication, by flash sintering, of a sintered body for use in a thermoelectric module. Gas-atomized Fe_2VAl powder was sintered with a current feed, for a duration on the order of seconds, using an apparatus specially devised for flash sintering. This produced sintered bodies in columnar form, with a diameter and height on the order of millimeters, which can be used for constructing thermoelectric modules without the need for a machining process, such as cutting or dicing. Although a slight reduction in density is observed, the crystal structure is unaffected by rapid heating and cooling. The magnitude of electrical and thermal conductivity is reduced, while the value of Seebeck coefficient is identical to that of a sample sintered by using conventional current sintering at 1373 K for 10 min. The significantly shorter sintering time can reduce energy consumption to less than 1 Wh, compared with the several hundred Wh required for conventional current sintering. Although it is still necessary to optimize the sintering conditions to overcome the reduction in density, the significant energy-conservation benefits of flash sintering have great practical appeal, especially for fabricating sintered bodies constituting thermoelectric power generation devices used for energy recovery.

Key words: Electric current activated/assisted sintering, flash sintering, thermoelectric material, Heusler alloy

INTRODUCTION

Thermoelectric (TE) energy conversion has been regarded as a promising technology for the effective use of energy resources. In particular, TE power generation is expected to be widely applied to recover energy from vast amounts of low-temperature waste heat, such as that below 600 K. The efficiency of TE conversion systems depends strongly on the performance of the TE materials, which is evaluated using a thermoelectric figure of merit, $ZT = S^2\sigma/\kappa$, where S is the Seebeck coefficient, σ the electrical conductivity, κ the thermal conductivity, and T the absolute temperature. TE materials with a high ZT value are required for the practical application of efficient TE energy conversion. In this regard, the Bi-Te alloys are known to be among the most effective TE materials. With a high ZT value of around 1 near room temperature,[1] this alloy can be used to construct TE devices having good energy conversion efficiency at low temperatures. However, in practice, the widespread use of Bi-Te TE devices has encountered difficulties due to higher costs and limited sources of raw materials. Moreover, it is difficult to construct a durable TE device using Bi-Te alloys because of their low oxidation resistance and poor mechanical strength.

The Heusler-type Fe_2VAl alloy is expected to be suitable for TE power generation near room temperature because of its large power factor PF

(Received May 16, 2019; accepted October 17, 2019; published online October 29, 2019)

(= $S^2\sigma$), such as 5.4 mW/mK^2 at 300 K.[2] In the Fe_2VAl system, by virtue of its electronic band structure with a sharp pseudo-gap around the Fermi-level,[3,4] high PF values for both *p*-type and *n*-type materials can be obtained by the control of valence electron concentration, such as Ti substitution for the V site for *p*-type, and Si substitution for the Al site for *n*-type.[2,5] Therefore, a TE module consisting solely of Fe_2VAl alloy can be fabricated, which is beneficial in relieving thermal stress on TE power generation. Furthermore, the high mechanical strength and the excellent chemical stability of this alloy are advantages in the construction of a durable TE module that can be used in harsh environments, such as the exhaust pipes of automobiles.[6] Moreover, the Fe_2VAl alloy consists of abundant and inexpensive elements, such as Fe and Al, which is also advantageous in producing low-cost TE devices on a large scale. Therefore, although the *ZT* value of the Fe_2VAl alloy of around 0.1–0.3[7] is lower than that of high-performance TE materials, such as Bi-Te alloy, because of its relatively high κ,[8] it promises to be useful in the high-volume production of durable TE power generation systems at low cost. Since there are some potential TE applications where durability and cost are prioritized over efficiency, such as the TE power generation for the exhaust heat from internal-combustion vehicles, we believe that the Fe_2VAl TE module holds possibilities for practical use.

For the construction of TE modules, sintered material having a fine microstructure is suitable because the artificially introduced microstructures, such as grain boundaries, interfaces and defects, can effectively reduce κ by the enhancement of phonon scattering, resulting in higher ZT values.[9–11] In addition, a reduction of the grain size also contributes to enhanced mechanical strength, which is an important consideration for constructing a durable TE device. For this purpose, a powder metallurgical process is a useful way to prepare the sintered materials, and electric current activated/assisted sintering (ECAS, also known as spark plasma sintering (SPS)) is a particularly effective means of controlling the microstructure, because of the rapid densification of the fine-grained powder in which grain growth is limited by abrupt heating/cooling under mechanical pressure.[12–14] In the past few decades, it has been demonstrated with a number of material studies that the microstructural modification by ECAS have efficacy for improving the TE performance.[15–17] In the case of Fe_2VAl alloy, we fabricated a microstructured Fe_2VAl sintered body by ECAS from pulverized alloy powder consisting of nanometer-sized crystallite prepared by mechanical alloying, and demonstrated that the enhanced phonon scattering at grain boundaries effectively reduced κ without deterioration in σ,[18] although the magnitude of κ was still several times higher than that of the state-of-the-art Bi-Te alloy.

As the next step toward practical implementation, the development of a high-volume production technique is required, because laboratory-scale equipment, such as planetary ball milling for powder preparation and time-consuming ECAS for sintering of centimeter-sized pellets, is inadequate for large-scale production. Therefore, the present study examined the use of Fe_2VAl alloy powder prepared by the gas atomization method, capable of kilogram-scale manufacturing, combined with flash sintering (FS), which can be defined as sintering with a duration on the order of seconds,[19] to sinter the Fe_2VAl TE legs. We recently investigated the use of FS for TE materials, and found that the TE material Sb_2Te_3 , with a typical size of Ø10 mm × 2 mm thick, could be obtained by ECAS with a duration of only a few seconds.[20] This result suggested that the minutes-long processing duration for conventional ECAS could be significantly shortened; moreover, the energy consumption for the sintering process could be reduced to less than 1% of that required for conventional ECAS.[20] This paper reports the results we obtained by using this newly developed sintering technique to directly fabricate final-form Fe_2VAl TE legs, which can be employed, without further machining processes such as cutting or dicing, in constructing a TE module. The sintering conditions necessary for preparing Fe_2VAl alloy for TE legs with a duration on the order of seconds were examined using finite element method (FEM) analysis. Then, gas-atomized Fe_2VAl alloy powder was sintered with a current feed duration on the order of seconds, using equipment specially developed for FS, and the TE properties were evaluated.

EXPERIMENTAL

Using COMSOL Multiphysics software, FEM analyses were conducted with a two-dimensional axisymmetric geometry in the time-dependent mode to enable the estimation of the sample temperature distribution during ECAS. The configured sample measured Ø5 mm × 5 mm thick, which is almost the same shape of the Fe_2VAl TE legs used for constructing a TE module in a previous study.[6] Assuming that ECAS would be conducted under vacuum, the boundary condition of the surfaces was assigned thermal radiation values, except for the top and bottom surfaces of the copper electrode, which had heat transfer coefficients of 10000 W/m^{2}K, assuming water cooling. The influence of the heating rate on the temperature distribution of the sample was examined. For simplicity, the temperature dependence of the material properties, shrinkage behavior, and Seebeck/Peltier effects were not taken into account. Under these conditions, the current needed to heat the sample center to 1273 K in a given period, t_s, was sought, and the temperature distribution within the sample was investigated.

Using specially developed FS equipment,[20] gas-atomized Ti-substituted Fe_2VAl powder with particle size < 250 μm (Daido Steel Co., Ltd.) was sintered in a vacuum (< 10 Pa) under a uniaxial pressure of 0.5 kN, using a stabilized zirconia mold and tungsten punch. In order to cancel out the Seebeck/Peltier effect by feeding current through the TE materials, a 100 Hz alternating current with a trapezoidal waveform was applied. Samples of the sintered alloy were fabricated in sizes of Ø5 mm × 4–6 mm height and Ø3 mm × 2–6 mm height, which are the typical dimensions of TE legs employed in TE modules. Using the Ø3 mm × 4 mm height sintered alloy sample, σ, κ and S were evaluated along the height direction. Because the small sample size made it difficult to accurately evaluate the TE properties, the average σ, κ and S values were estimated by measuring six different FSed alloys with the same sintering condition of 1.2 kA/0.5 s. For comparison, a conventional ECAS machine (LABOX-625FC, Sinter Land, Inc.) was used to sinter the same Fe_2VAl powder at 1323 K for 1 min and 1373 K for 10 min in a vacuum under a uniaxial pressure of 50 MPa, using a graphite mold and punch. In this case, the heating and cooling rates were both 100 K/min. The obtained bulk samples, with a typical size of Ø10 mm × 2 mm thick, were first used to acquire the value of κ and were then cut into bar shapes with a typical size of 2 mm × 2 mm × 9 mm for measuring σ and S.

Crystalline phase analysis was performed using x-ray diffraction (XRD) with Cu Kα radiation. Microstructural observation was conducted using scanning electron microscopy (SEM). For the Ø10 mm samples prepared by conventional ECAS, S and σ were simultaneously measured in a He atmosphere using an electrical conductivity and Seebeck coefficient measurement system (RZ2001i, Ozawa Science Co., Ltd.). Further, κ was evaluated from the density (D), thermal diffusivity (α), and specific heat (C_p), given the relationship $\kappa = D \times \alpha \times C_p$. Here, D was calculated from the volume and weight of the specimens, and α and C_p were evaluated using the laser-flash method (LFA457, NETZSCH-Gerätebau GmbH). For the Ø3 mm sample prepared by FS, σ, κ and S were separately measured only at room temperature using the homemade apparatus, because the sample was too small to be attached to the conventional measuring apparatus, such as RZ2001i. The value of σ was calculated from the sample size and the slope of current–voltage plot measured by means of a conventional four-probe DC technique with the positive and negative current flow along the sample height direction. The value of S was calculated by plotting the thermoelectric voltage versus the temperature difference of 0–5 K along the sample height direction. The value of κ was evaluated by a steady-state comparative-longitudinal heat flow method[21] under vacuum with a reference material of Inconel 600 (13.9 W/mK) at a temperature difference around 2 K.

RESULTS AND DISCUSSION

The uniform heating of a sample is apparently one of the most important conditions for the sintering process. Therefore, the temperature distribution as a function of heating rate was examined by FEM analysis. Since mechanical pressure is indispensable for the densification and the microstructure refinement of Fe_2VAl sintered alloy, ECAS with sintering die and punch was examined. As shown in Fig. 1a, a configuration anticipated for Fe_2VAl sintering was constructed, using the components having physical properties listed in Table I. Note that a non-conductive zirconia die and a highly conductive tungsten punch were used in our model, whereas a graphite die and punch are usually employed for ECAS. As discussed in the previous study, the insulating mold is indispensable to achieve a high level of temperature uniformity along the vertical direction, resulting from a homogenous Joule-heating effect.[20] The difference in the heating effect between the tungsten punch and the graphite punch on the temperature distribution will be discussed with the FEM results below. In addition, in order to avoid heat loss from the sample to the punch, and to prevent reaction between Fe_2VAl and tungsten, graphite sheets with anisotropic transport properties were inserted between the sample and the punch. Using this model, temperature uniformity within the sample when the sample center was heated to 1273 K in a given period, t_s, was examined.

As shown in Fig. 1b, when t_s was on the order of minutes (e.g., 1000 s), radial temperature distribution was observed extending from the sample center, resulting in non-uniform temperature distribution in the inside of the sample. Then, decreasing t_s, corresponding to an increase in the heating rate, reduced the extent of the heating, thereby increasing the non-uniformity of the sample temperature distribution until $t_s \approx 1$ s. Usually, this temperature non-uniformity can be avoided by using a graphite punch, which can generate a higher Joule-heating effect than a tungsten punch because of its higher electrical resistance. Replacement of the tungsten punch by a graphite punch (see Fig. 1c of 1000 s) enabled the high-temperature region to be extended, resulting in a highly homogeneous temperature distribution inside the sample sintered over a period of minutes. However, our work to refine the FS method showed the consequence of shortening t_s to less than 1 s to be that the higher Joule-heating effect of graphite would cause the punch to overheat, giving rise to a non-uniform temperature distribution within the sample (see Fig. 1c of 0.1 s). Without conducting FEM, it is apparent that a material with the same σ as the sample would be an ideal punch material; however,

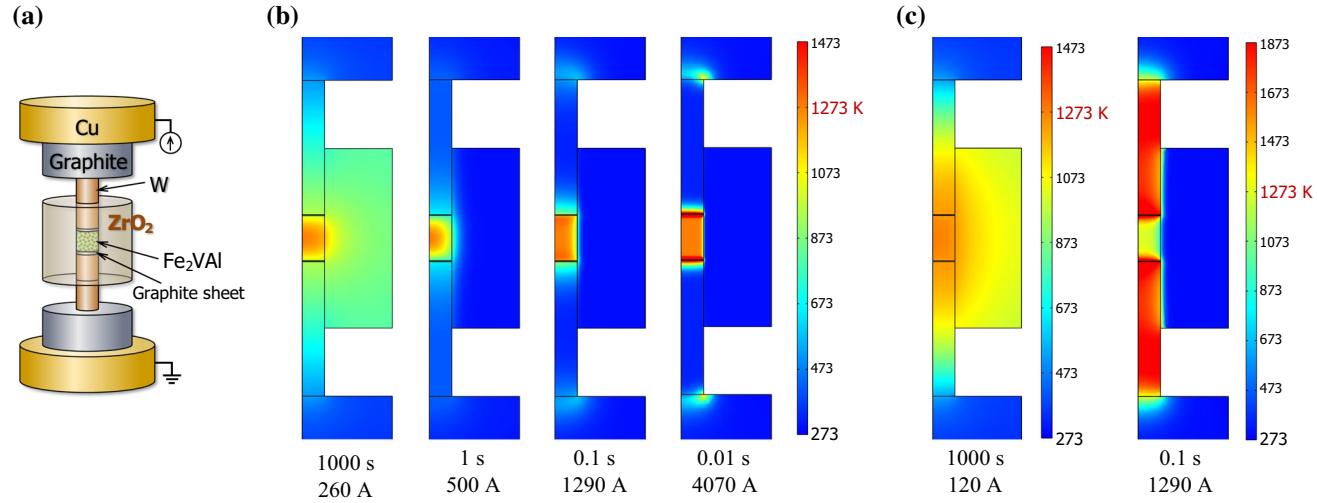

Fig. 1. (a) Configuration for FEM analysis of ECAS for near-net-shape sintering of Fe_2VAl alloy with a size of Ø5 mm × 5 mm height. (b) Calculated temperature distribution images when the sample center reaches 1273 K with different heating rates. (c) Calculated temperature distribution in the case of graphite punch.

Table I. Material parameters for FEM analysis

Material	D (kg/m^3)	σ (S/m)	C_p (J/kgK)	κ (W/mK)
Copper	8700	6×10^7	385	400
Graphite	1840	9×10^4	1600	60
Zirconia	6000	0	600	3.5
Tungsten	17800	5.5×10^6	145	130
Graphite sheet				
In-plane	2000	2.8×10^5	1600	240
Out-of-plane		1.2×10^4		7
Fe_2VAl	4500	1.5×10^5	650	8.5

no such ideal material was identified when taking into account the high mechanical strength and high resistance needed to withstand thermal shock.

Instead, the use of a tungsten punch and graphite sheets allowed the temperature uniformity within a sample to be enhanced. As shown in Fig. 1b, when t_s was further shortened (e.g., 0.1–0.01 s), the high-temperature area was limited to the sample in conjunction with the improvement of temperature uniformity within the sample. Although a slightly overheated area occurred around the graphite sheet when the heating rate was overly high (such as t_s = 0.01 s), the lower κ and σ of the graphite sheet along the out-of-plane direction could prevent heat loss from the sample to the tungsten punch and enhance the uniform heating of the sample. The dependence of the temperature distribution on the heating rate in the model based on the tungsten punch and zirconia die is summarized in Fig. 2. As mentioned above, when t_s was on the order of minutes (e.g., 1000 s), the high temperature area was extended to the mold by the heat transfer from the Joule-heating current path. Therefore, when t_s was reduced to 1 s, the heat loss from the Joule-

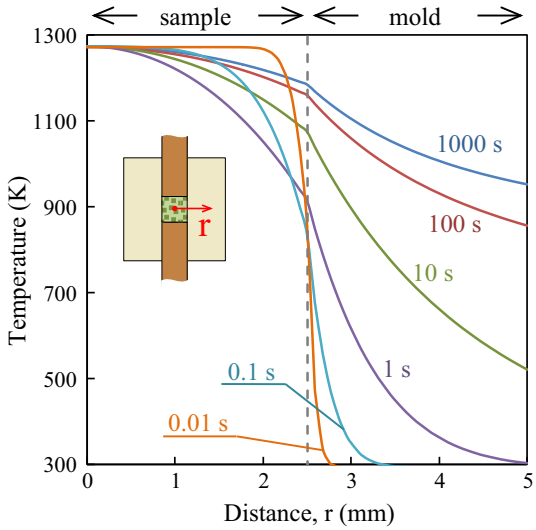

Fig. 2. Calculated temperature profiles along a horizontal line from the sample center (r = 0 mm) to radial direction for different heating rates by the FEM analysis.

heating sample to the non-heating insulating mold caused a large temperature gradient in a radial direction. However, if the heating rate was sufficiently high compared to the thermal diffusivity of the mold material (e.g., 1 mm^2/s for zirconia), the heat transfer effect on the temperature distribution became less effective and the high temperature area was confined to the Joule-heating area, resulting in the enhancement of temperature uniformity within the sample. Consequently, the FEM analysis suggested that uniform heating of the Fe_2VAl alloy could be achieved by accelerating the heating rate to 1000–10000 K/s with a current feed of 1–4 kA.

To validate the actual FS of the Fe_2VAl alloy, $Fe_2V_{0.9}Ti_{0.1}Al$ alloy powder was sintered using

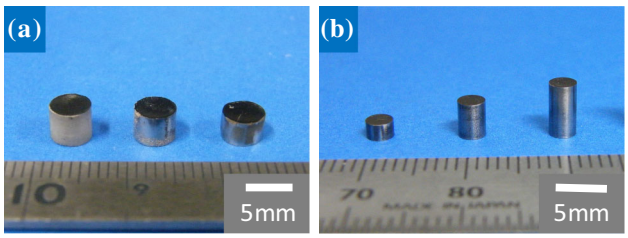

Fig. 3. Fe_2VAl sintered bodies prepared by flash sintering. (a) Ø5 mm × 5–3 mm height and (b) Ø3 mm × 2–6 mm height.

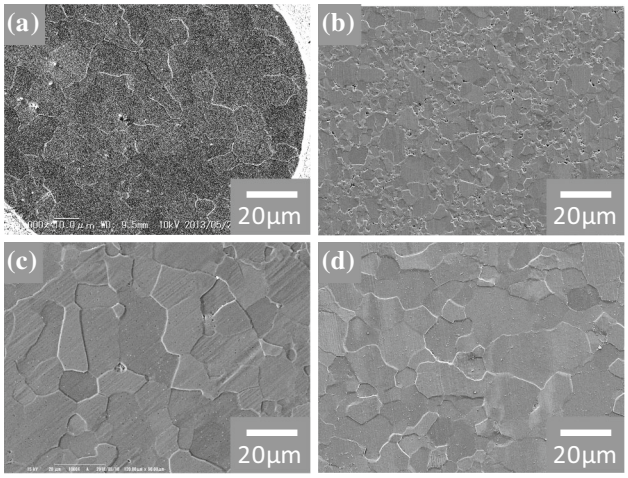

Fig. 4. SEM images of cross-sections of (a) gas-atomized $Fe_2V_{0.9}Ti_{0.1}Al$ powder, sintered sample prepared by conventional ECAS of (b) 1323 K/1 min, (c) 1373 K/10 min, and (d) FS of current feed of 1.2 kA for 0.5 s.

equipment that was specially designed for FS.[20] As the aim of this study was to develop a practical method for the high-volume production of Fe_2VAl TE legs, we used a Fe_2VAl alloy powder prepared by gas atomization, a method capable of kilogram-scale manufacturing. The FEM result suggested that FS for Fe_2VAl required extremely rapid sintering within 1 s; however, a conventional method to achieve feedback adjustment for sintering, such as PID temperature control, was not available. Therefore, the optimum duration and current (which remained constant during each individual sintering test) were sought through a trial-and-error approach. Consequently, as shown in Fig. 3, millimeter-sized sintered bodies were obtained with a current feed duration of 1.2 kA/0.5 s for Ø3 and 1.5 kA/2.0 s for Ø5. It was confirmed that the Fe_2VAl samples subjected to FS were uniformly densified in almost all parts of the sample, except for an outer rim around the edge, approximately 0.3 mm wide, which was directly in contact with the unheated zirconia mold. Then, the relative density of FSed sample reached 95.1%, although this value was lower than that of samples prepared by conventional ECAS of 1373 K/10 min of 99.9%. Noteworthy is that the energy consumption for the FS of Fe_2VAl

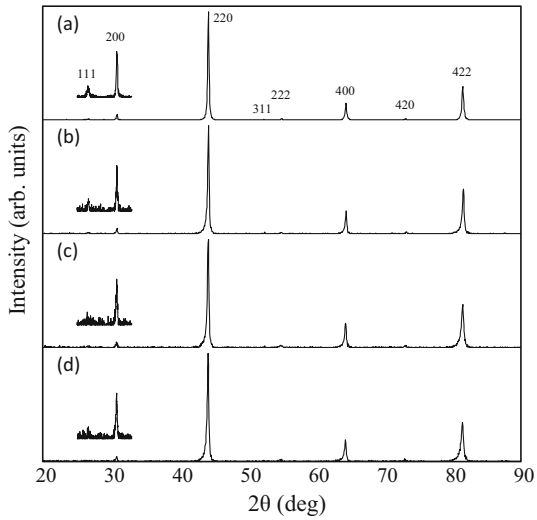

Fig. 5. XRD patterns (Cu Kα radiation) diffracted from (a) the gas-atomized $Fe_2V_{0.9}Ti_{0.1}Al$ powder and a sintered sample prepared by conventional ECAS of (b) 1323 K/1 min, (c) 1373 K/10 min, and (d) FS of current feed of 1.2 kA for 0.5 s.

alloys was approximately 1 Wh or less, which is considerably lower than the several hundred Wh consumption for the conventional ECAS with a duration on the order of minutes. From a practical viewpoint, this significant reduction of energy consumption for the sintering process should be appealing, especially for fabricating the TE legs used for power generation applications and aimed at energy recovery.

The microstructure of the sintered alloys is shown in Fig. 4. Interestingly, sintering the gas-atomized Fe_2VAl powder under conventional ECAS conditions of 1323 K for 1 min led to a reduction in the original grain size of approximately 9 μm of gas-atomized powder (Fig. 4a) to 2.5 μm (Fig. 4b) due to the effect of plastic deformation during the initial stage of the sintering process. This result implies that ECAS associated with mechanical pressure could be a beneficial means of microstructural refinement, even when the original powder is not sufficiently refined. On the other hand, an increase in the sintering temperature and duration time, namely ECAS of 1373 K for 10 min (Fig. 4c), caused the grain size to increase to 11 μm because of the regrowth of crystal grains with structural rearrangement by atomic diffusion in a solid occurring in the later stage of the sintering process. In the case of the FSed sample (Fig. 4d), the fact that the grain size approximated 10 μm seemed to indicate that a rapid densification process proceeded at temperatures of 1373 K or higher. Although a smaller grain size is desirable for the suppression of κ, the plastic deformation at lower temperatures, which seems to take minutes, could not be utilized for rapid FS with a duration of seconds. Therefore, FS required high-temperature conditions, at which Fe_2VAl could be readily deformed under mechanical

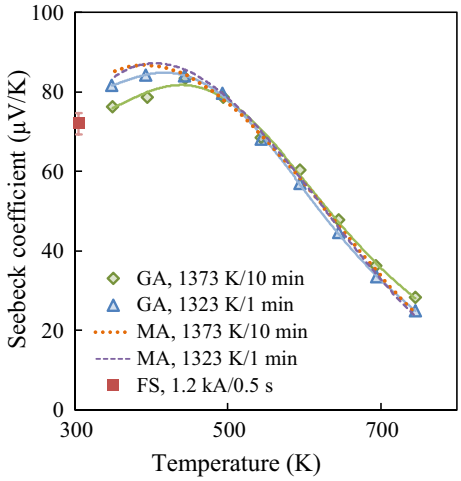

Fig. 6. Temperature dependence of Seebeck coefficient of sintered $Fe_2V_{0.9}Ti_{0.1}Al$ alloys. Samples were prepared by conventional ECAS from gas-atomized powder (GA), from mechanically alloyed powder (MA),[17] and prepared by FS from gas-atomized powder (FS).

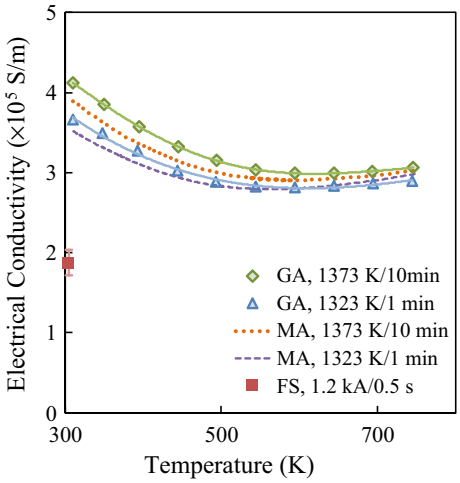

Fig. 7. Temperature dependence of electrical resistivity in sintered $Fe_2V_{0.9}Ti_{0.1}Al$ samples. Samples were prepared by conventional ECAS from gas-atomized powder (GA), from mechanically alloyed powder (MA),[17] and prepared by FS from gas-atomized powder (FS).

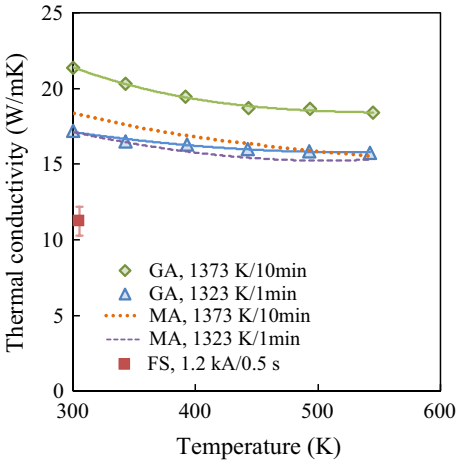

Fig. 8. Temperature dependence of thermal conductivity in sintered $Fe_2V_{0.9}Ti_{0.1}Al$ samples. Samples were prepared by conventional ECAS from gas-atomized powder (GA) and from mechanically alloyed powder (MA),[17] and prepared by FS from gas-atomized powder (FS).

pressure, and the constituent elements could rapidly diffuse. Higher mechanical pressure (on the scale of GPa) during sintering might reduce the time and temperature required for densification, and also might enhance microstructural refinement; however, such experiments could not be conducted with our present FS apparatus.

XRD measurements of the gas-atomized Fe_2VAl powder and the polished cross-section of Fe_2VAl sintered alloys were conducted to investigate the effect of sintering on the crystal structures of the obtained samples. Figure 5a shows the XRD pattern, which indicates that the gas-atomized Fe_2VAl powder forms a Heusler-type ($L2_1$) structure. Although the gas-atomized powder was rapidly cooled from the molten state by inert gas jets, this XRD result suggests that the gas atomization process could produce Fe_2VAl alloy powder with the $L2_1$ ordered crystallographic structure. The electronic band structure is closely related to the crystallographic structure, and the $L2_1$ ordering for the Fe_2VAl phase is particularly indispensable for the formation of a pseudogap across the Fermi level, which is the origin of the high TE performance of this alloy.[2,5] Therefore, the highly ordered crystal structure in gas-atomized powder is desirable for TE materials as well as the original powder for FS, because enhanced ordering of the crystallographic structure during FS is limited by the lower annealing effect of FS. As shown in Fig. 5, it was confirmed that all of the Fe_2VAl alloys that were sintered under different conditions formed the Heusler-type ($L2_1$) structure without an impurity phase. Furthermore, the differences in the 2θ angle of diffraction peaks between the FSed alloy and the samples prepared by conventional ECAS were negligibly small. Therefore, the estimated lattice parameter of a = 5.788 Å for the FS sample was almost the same as that of a = 5.785 Å for the conventional ECAS (1373 K/10 min) sampl,e and even that of a = 5.782 Å for the gas-atomized powder. These SEM and XRD observations indicate that a sintered Fe_2VAl alloy, which possesses qualities similar to those of samples prepared by the conventional ECAS, could be obtained by FS.

Finally, the TE properties of the sintered alloys were evaluated to examine the effect of FS on the TE performance. For comparison, the TE properties of the sintered Fe_2VAl alloy with sub-micrometer grain size, prepared from mechanically alloyed powder with nanometer-sized crystallites,[18] are indicated as dashed lines in Figs. 6, 7 and 8. As shown in Fig. 6, the sintered alloys produced from gas-atomized alloy powder with conventional ECAS

Table II. ZT values of Fe_2VAl sintered alloys. ZT at 350 K for ECAS samples and at 300 K for FS sample

Powder	GA			MA	
	ECAS		FS	ECAS	
Sintering condition	1323 K/1 min	1373 K/10 min	1.2 kA/0.5 s	1323 K/1 min	1373 K/10 min
ZT value	0.05	0.04	0.03	0.05	0.05

exhibited almost the same S value as that of the sintered alloy made from mechanically alloyed powder. Furthermore, the FSed alloy also exhibited a similar S value when the temperature dependence of S in $Fe_2V_{0.9}Ti_{0.1}Al$ alloy[5,22] was taken into account. Because the value of S is governed by the electronic density of states around the Fermi level and the carrier density, its magnitude and temperature dependence are highly affected by the crystallographic structure and chemical composition, while being less affected by the microstructure. Especially for the Heusler Fe_2VAl alloy, the degree of $L2_1$ ordering of the crystal structure significantly affects the S value. Therefore, this result for the value of S indicates that sintered alloys with the same quality of the Heusler Fe_2VAl phase could be obtained, irrespective of the method that was used to prepare the original powder and the sintering rate. This finding is consistent with the above-mentioned XRD analysis results.

In contrast to the result of S, since the transport properties σ and κ are highly sensitive to the microstructure, those values vary in magnitude, as shown in Figs. 7 and 8. In the case of the sintered alloys prepared by conventional ECAS, the difference in the σ value could be caused by the differing grain size resulting from the different amount of carrier transport scattering at grain boundaries. Therefore, enhancing the grain growth by using a higher sintering temperature, such as 1373 K for 10 min, could increase the σ value. Conversely, the FSed alloys had a much lower σ value, although the grain size was as large as that of the alloy prepared by conventional ECAS at 1373 K/10 min. The reduction in σ may be caused by the lower density of the FSed alloy, especially for an outer rim around the edge, which was directly in contact with the unheated zirconia mold during FS. In addition, because it seems reasonable to suppose that the surface of the gas-atomized powder is slightly oxidized during powder treatment in air, the oxidation layer would remain in the FSed sample, whereas the oxidized part could be dispersed and removed by the longer heat treatment in the reducing atmosphere of the graphite mold in the case of conventional ECAS. Although a more detailed evaluation is needed, it may be assumed that the lower density and the remaining insulating oxidation layer might account for the lower σ in FSed Fe_2VAl alloy.

As shown in Fig. 8, a similar microstructure dependence was observed in the magnitude of the κ value. The sample obtained by FS exhibited a much lower κ value compared to the samples prepared by ECAS, as in the case of σ. Consequently, the negative effect of the decrease in σ of FSed alloy for TE performance could be almost compensated by the decrease in κ. The reduction in κ of FSed alloy might also be caused by the lower density. However, even if the effect of porosity was taken into account, the measured value of 11.2 W/mK was much lower than the estimated value of 19.8 W/mK derived from the Maxwell's formula for calculating the κ value of porous materials, assuming that 21.4 W/mK of the sample prepared by the conventional ECAS of 1373 K/10 min was the κ value for the fully densified specimen.[23] Therefore, additional scattering factors might affect phonon transport in the FSed sample, such as crystal lattice distortion induced by rapid heating/cooling and the remained oxidation layer, as mentioned above.

For the samples prepared by conventional ECAS, as expected from the microstructure previously shown in Fig. 4, the reduction in grain size by plastic deformation at lower temperatures (which occurred in the sintered sample prepared from gas-atomized powder by ECAS of 1323 K/1 min, Fig. 4b) could contribute to the suppression of κ, comparable to the sub-micrometer order of grain size reduction, such as in the sintered alloy prepared from mechanically alloyed powder by ECAS of 1323 K/1 min. This result further suggests that the ECAS process might provide an effective means of controlling the microstructure and transport properties, even if the microstructure of the starting powder is not sufficiently refined. In addition, from a practical perspective, this result indicates that laboratory-scale powder preparation at the gram scale using methods such as mechanical alloying could be replaced by a method capable of high-volume powder preparation, e.g., gas atomization, without degradation of the TE performance. Finally, ZT value of sintered Fe_2VAl alloys were calculated and listed in Table II. Even if the lower T and the temperature dependence of S in $Fe_2V_{0.9}Ti_{0.1}Al$ were taken into account, the ZT value of FSed sample is lower than that of samples prepared by conventional ECAS mainly because of the degradation of σ. Therefore, for the improvement of σ, the elimination of pores by the

optimization of sintering condition or the pretreatment of the gas-atomized power, such as the control of particle size or the removal of the surface oxidation layer, will be the next step for the further investigations.

CONCLUSION

The flash sintering of Fe_2VAl alloy samples at sizes typically utilized for components in thermoelectric modules was examined by FEM analysis. In addition, the sintering of these samples with a duration on the order of seconds was experimentally evaluated. The FEM analysis for zirconia die and tungsten punch model suggests that uniformity of temperature distribution could be enhanced by a sufficiently accelerated Joule-heating rate, compared to the thermal diffusion rate of the zirconia die. Evaluation of the FSed Fe_2VAl alloys demonstrated that the crystal structure was unchanged after the rapid heating/cooling with sintering shrinkage, while a remainder of insufficiently densified material was observed at an outer rim around the edge. Consequently, the magnitude of σ and κ with the whole volume of the FSed sample was reduced, whereas the S value remained unchanged. Because the negative effect of the decrease in σ on TE properties could be almost compensated by the same level of decrease in κ, the TE performance of sintered alloy prepared by ECAS could be reproduced by FS. Although the optimization of FS conditions and treatment of the original powder for the enhancement of densification require further investigation, the significant reduction in process duration and energy consumption (< 1 Wh, compared with several hundred Wh for conventional ECAS) is expected to be appealing from a practical viewpoint, especially for fabricating thermoelectric materials used for power generation and aimed at energy recovery.

ACKNOWLEDGMENTS

This work was partly supported by the Adaptable and Seamless Technology Transfer Program through Target-driven R&D, A-STEP (No. AS2415009L), Japan Science and Technology Agency, JST.

REFERENCES

1. D.M. Rowe, *CRC Handbook of Thermoelectrics* (Boca Raton: CRC Press, 1995).
2. H. Kato, M. Kato, Y. Nishino, U. Mizutani, and S. Asano, *J. Jpn. Inst. Metals* 65, 652 (2001).
3. D. Singh and I. Mazin, *Phys. Rev. B - Condens. Matter Mater. Phys.* 57, 14352 (1998).
4. R. Weht and W. Pickett, *Phys. Rev. B - Condens. Matter Mater. Phys.* 58, 6855 (1998).
5. H. Matsuura, Y. Nishino, U. Mizutani, and S. Asano, *J. Jpn. Inst. Metals* 66, 767 (2002).
6. M. Mikami, M. Mizoshiri, K. Ozaki, H. Takazawa, A. Yamamoto, Y. Terazawa, and T. Takeuchi, *J. Electron. Mater.* 43, 1922 (2014).
7. S. Masuda, K. Tsuchiya, J. Qiang, H. Miyazaki, and Y. Nishino, *J. Appl. Phys.* 124, 035106 (2018).
8. Y. Nishino, S. Deguchi, and U. Mizutani, *Phys. Rev. B* 74, 115115 (2006).
9. Y. Lan, A.J. Minnich, G. Chen, and Z. Ren, *Adv. Funct. Mater.* 20, 357 (2010).
10. K. Nielsch, J. Bachmann, J. Kimling, and H. Böttner, *Adv. Energy Mater.* 1, 713 (2011).
11. K. Biswas, J. He, I.D. Blum, C.I. Wu, T.P. Hogan, D.N. Seidman, V.P. Dravid, and M.G. Kanatzidis, *Nature* 489, 414 (2012).
12. S. Grasso, Y. Sakka, and G. Maizza, *Sci. Technol. Adv. Mater.* 10, 053001 (2009).
13. R. Orru, R. Licheri, A.M. Locci, A. Cincotti, and G. Cao, *Mater. Sci. Eng., R* 63, 127 (2009).
14. O. Guillon, J. Gonzalez-Julian, B. Dargatz, T. Kessel, G. Schierning, J. Rathel, and M. Herrmann, *Adv. Eng. Mater.* 16, 830 (2014).
15. W.S. Liu, B.P. Zhang, J.F. Li, H.L. Zhang, and L.D. Zhao, *J. Appl. Phys.* 102, 103717 (2007).
16. M. Scheele, N. Oeschler, K. Meier, A. Kornowski, C. Klinke, and H. Weller, *Adv. Funct. Mater.* 19, 3476 (2009).
17. B. Du, F. Gucci, H. Porwal, S. Grasso, A. Mahajan, and M.J. Reece, *J. Mater. Chem. C* 5, 1514 (2017).
18. M. Mikami, Y. Kinemuchi, K. Ozaki, Y. Terazawa, and T. Takeuchi, *J. Appl. Phys.* 111, 093710 (2012).
19. M. Yu, S. Grasso, R. Mckinnon, T. Saunders, and M.J. Reece, *Adv. Appl. Ceram.* 116, 24 (2017).
20. M. Mikami, Y. Kinemuchi, K. Kubo, N. Uchiyama, H. Miyazaki, and Y. Nishino, *J. Appl. Phys.* 124, 105104 (2018).
21. D. Zhao, X. Qian, X. Gu, S.A. Jajja, and R. Yang, *J. Electron. Packag.* 138, 040802 (2016).
22. T. Mori, N. Ide, and Y. Nishino, *J. Jpn. Inst. Metals* 72, 593 (2008).
23. J.C. Maxwell, *A Treatiseon Electricity and Magnetism*, Vol. 365 (Oxford: Clarendon Press, 1873).